SUPPLEMENTARY INFORMATION: PHASE-CONTROLLED NON-MARKOVIAN HYSTERESIS IN A NONLINEAR, NON-HERMITIAN SILICON MICRORESONATOR

RESEARCH ARTICLE

Stefano Biasi*, **Stefano Gretter*,** **Bülent Aslan,** **Davide Olivieri,** **Riccardo Franchi,** **Lorenzo Pavesi**

Nanoscience Laboratory, Department of Physics, University of Trento, 38123 Trento, Italy

*These authors contributed equally
Corresponding authors: stefano.biasi@unitn.it

August 12, 2025

1 Linear regime: analytical response of DRUM

In this section, we obtain an explicit analytical expression for the time dependence of the complex optical field amplitudes (α_1 and α_2) of the DRUM in the linear regime. We refer to Fig. 2(a) of the main text for the actual design of the DRUM and the definition of the two optical modes. As shown in [1], using the Temporal Coupled Mode Theory (TCMT) we obtain:

$$\begin{aligned}\frac{d\alpha_1}{dt} &= \left(i(\omega_\mathrm{r}-\omega)-\frac{\gamma_\mathrm{loss}}{2}\right)\alpha_1-\beta_{21}\alpha_2\\ \frac{d\alpha_2}{dt} &= \left(i(\omega_\mathrm{r}-\omega)-\frac{\gamma_\mathrm{loss}}{2}\right)\alpha_2-\beta_{12}\alpha_1+i\sqrt{\gamma_\mathrm{coup}}E_\mathrm{in},\end{aligned} \tag{1}$$

where ω_r is the resonant angular frequency, ω is the laser angular frequency, and γ_loss is the total loss rate (i.e. the sum of intrinsic $\gamma_\mathrm{rad}+\gamma_\mathrm{abs}$ and extrinsic losses $5\gamma_\mathrm{coup}$, since there are five coupling points in the DRUM), and β_{12} and β_{21} are the complex coupling coefficients. Specifically, β_{12} accounts for the energy exchange from α_1 to α_2, while β_{21} accounts for the reverse exchange from α_2 to α_1. We note that this notation is consistent with that used in reference [1], by using the following relations: $\frac{\gamma_\mathrm{loss}}{2}=\gamma_t$, and $\gamma_\mathrm{coup}=2\Gamma_0$. The Jacobian of the system takes the following form:

$$\mathcal{J}=\begin{pmatrix} i\left(\omega_\mathrm{r}-\omega\right)-\frac{\gamma_\mathrm{loss}}{2} & -\beta_{21}\\ -\beta_{12} & i\left(\omega_\mathrm{r}-\omega\right)-\frac{\gamma_\mathrm{loss}}{2}\end{pmatrix}. \tag{2}$$

As a result, the eigenvalues are:

$$\lambda_{1,2}=i\left(\omega_\mathrm{r}-\omega\right)-\frac{\gamma_\mathrm{loss}}{2}\mp\sqrt{\beta_{21}\beta_{12}}, \tag{3}$$

and the non-normalized eigenvectors are reduced as:

$$\vec{\xi}_{1,2}=\begin{pmatrix}\pm\frac{\sqrt{\beta_{12}\beta_{21}}}{\beta_{12}}\\ 1\end{pmatrix}. \tag{4}$$

To obtain the explicit solution of equation 1, we first rewrite it in a matrix form as:

$$\vec{x}'=\mathcal{J}\vec{x}+\vec{f}, \tag{5}$$

where:

$$\vec{x} = \begin{pmatrix} \alpha_1 \\ \alpha_2 \end{pmatrix}, \tag{6}$$

$$\vec{f} = \begin{pmatrix} 0 \\ i\sqrt{\gamma_{\text{coup}}}E_{\text{in}} \end{pmatrix}, \tag{7}$$

$$\vec{x}_0 = \begin{pmatrix} \alpha_{1,0} \\ \alpha_{2,0} \end{pmatrix}. \tag{8}$$

In this mathematical framework, $\vec{x}_0$ is defined as the initial state at time $t = 0$ of α_1 and α_2. As a result, the eigenvectors matrix can be written as:

$$\underline{e} = \begin{pmatrix} \frac{\sqrt{\beta_{12}\beta_{21}}}{\beta_{12}} & -\frac{\sqrt{\beta_{12}\beta_{21}}}{\beta_{12}} \\ 1 & 1 \end{pmatrix} \Rightarrow \underline{e}^{-1} = \begin{pmatrix} \frac{\beta_{12}}{2\sqrt{\beta_{12}\beta_{21}}} & \frac{1}{2} \\ -\frac{\beta_{12}}{2\sqrt{\beta_{12}\beta_{21}}} & \frac{1}{2} \end{pmatrix}. \tag{9}$$

Then, let us formulate the term $\vec{f}$ as a combination of the eigenvectors:

$$\vec{f} = g_1\vec{\xi_1} + g_2\vec{\xi_2}, \tag{10}$$

where:

$$\begin{pmatrix} g_1 \\ g_2 \end{pmatrix} = \underline{e}^{-1}\vec{f} = \begin{pmatrix} \frac{i\sqrt{\gamma_{\text{coup}}}E_{\text{in}}}{2} \\ \frac{i\sqrt{\gamma_{\text{coup}}}E_{\text{in}}}{2} \end{pmatrix}. \tag{11}$$

Similarly, we can derive an expression for $\vec{x}_0$:

$$\begin{aligned} &\vec{x}_0 = a_1\vec{\xi_1} + a_2\vec{\xi_2} \\ &\Rightarrow \begin{pmatrix} a_1 \\ a_2 \end{pmatrix} = \underline{e}^{-1}\vec{x}_0 = \begin{pmatrix} \frac{\beta_{12}}{2\sqrt{\beta_{12}\beta_{21}}} & \frac{1}{2} \\ -\frac{\beta_{12}}{2\sqrt{\beta_{12}\beta_{21}}} & \frac{1}{2} \end{pmatrix}\begin{pmatrix} \alpha_{1,0} \\ \alpha_{2,0} \end{pmatrix} = \begin{pmatrix} \frac{\alpha_{2,0}}{2} + \frac{\beta_{12}\alpha_{1,0}}{2\sqrt{\beta_{12}\beta_{21}}} \\ \frac{\alpha_{2,0}}{2} - \frac{\beta_{12}\alpha_{1,0}}{2\sqrt{\beta_{12}\beta_{21}}} \end{pmatrix}, \end{aligned} \tag{12}$$

while $\vec{x}$, and $\vec{x}'$ can be written as a combination of the eigenvectors:

$$\begin{aligned} \vec{x} &= x_1\vec{\xi_1} + x_2\vec{\xi_2} \\ \vec{x}' &= x_1'\vec{\xi_1} + x_2'\vec{\xi_2}. \end{aligned} \tag{13}$$

By substituting equation 13 and equation 10 into equation 5, we obtain:

$$x_1'\vec{\xi_1} + x_2'\vec{\xi_2} = \mathcal{J}(x_1\vec{\xi_1} + x_2\vec{\xi_2}) + g_1\vec{\xi_1} + g_2\vec{\xi_2}. \tag{14}$$

Finally, using relation $\mathcal{J}\vec{\xi_i} = \lambda_i\vec{\xi_i}$, we can write the following expression:

$$x_1'\vec{\xi_1} + x_2'\vec{\xi_2} = x_1\lambda_1\vec{\xi_1} + x_2\lambda_2\vec{\xi_2} + g_1\vec{\xi_1} + g_2\vec{\xi_2}, \tag{15}$$

which may be solved independently for the coefficients multiplying the two eigenvectors: $\xi_i' = \xi_i\lambda_i + g_i$. One can solve these equations with the integrating factor as:

$$\begin{aligned} x_i &= C_i e^{\lambda_i t} + e^{\lambda_i t}\int g_i e^{-\lambda_i t}\, dt \\ &= C_i e^{\lambda_i t} - \frac{g_i}{\lambda_i}. \end{aligned} \tag{16}$$

Finally, by fixing the integrating constants with the initial conditions:

$$\begin{aligned} a_i = x_i(0) &= C_i - \frac{g_i}{\lambda_i} \\ \Rightarrow C_i &= a_i + \frac{g_i}{\lambda_i}, \end{aligned} \tag{17}$$

we can insert equation 16 and 17 in equation 13 to get:

$$\begin{aligned} \vec{x} = x_1\vec{\xi_1} + x_2\vec{\xi_2} &= \left(C_1 e^{\lambda_1 t} - \frac{g_1}{\lambda_1}\right)\vec{\xi_1} + \left(C_2 e^{\lambda_2 t} - \frac{g_2}{\lambda_2}\right)\vec{\xi_2} \\ &= \left[\left(a_1 + \frac{g_1}{\lambda_1}\right)e^{\lambda_1 t} - \frac{g_1}{\lambda_1}\right]\vec{\xi_1} + \left[\left(a_2 + \frac{g_2}{\lambda_2}\right)e^{\lambda_2 t} - \frac{g_2}{\lambda_2}\right]\vec{\xi_2}. \end{aligned}$$

Rewriting the previous expression explicitly, we obtain the final solution:

$$\begin{aligned}
\alpha_1 = &\left[\left(\frac{\alpha_{2,0}}{2}\frac{\sqrt{\beta_{12}\beta_{21}}}{\beta_{12}} + \frac{\alpha_{1,0}}{2} + \frac{\sqrt{\beta_{12}\beta_{21}}i\sqrt{\gamma_{\text{coup}}}E_{\text{in}}}{2\beta_{12}\lambda_1}\right)e^{\lambda_1 t} - \frac{\sqrt{\beta_{12}\beta_{21}}i\sqrt{\gamma_{\text{coup}}}E_{\text{in}}}{2\beta_{12}\lambda_1}\right] \\
&- \left[\left(\frac{\alpha_{2,0}}{2}\frac{\sqrt{\beta_{12}\beta_{21}}}{\beta_{12}} - \frac{\alpha_{1,0}}{2} + \frac{\sqrt{\beta_{12}\beta_{21}}i\sqrt{\gamma_{\text{coup}}}E_{\text{in}}}{2\beta_{12}\lambda_2}\right)e^{\lambda_2 t} - \frac{\sqrt{\beta_{12}\beta_{21}}i\sqrt{\gamma_{\text{coup}}}E_{\text{in}}}{2\beta_{12}\lambda_2}\right] \\
\alpha_2 = &\left[\left(\frac{\alpha_{2,0}}{2} + \frac{\alpha_{1,0}}{2}\frac{\beta_{12}}{\sqrt{\beta_{12}\beta_{21}}} + \frac{i\sqrt{\gamma_{\text{coup}}}E_{\text{in}}}{2\lambda_1}\right)e^{\lambda_1 t} - \frac{i\sqrt{\gamma_{\text{coup}}}E_{\text{in}}}{2\lambda_1}\right] \\
&+ \left[\left(\frac{\alpha_{2,0}}{2} - \frac{\alpha_{1,0}}{2}\frac{\beta_{12}}{\sqrt{\beta_{12}\beta_{21}}} + \frac{i\sqrt{\gamma_{\text{coup}}}E_{\text{in}}}{2\lambda_2}\right)e^{\lambda_2 t} - \frac{i\sqrt{\gamma_{\text{coup}}}E_{\text{in}}}{2\lambda_2}\right]
\end{aligned} \tag{18}$$

For times $t \to \infty$, this expression reduces to the typical steady-state spectral response shown in [1]. The transmission, formalized as $t_r = 1 + i\sqrt{\gamma_{coup}}\,\alpha_2/E_{\text{in}}$, can take different shapes depending on the values of the coupling coefficients $\beta_{i,j}$, ranging from a single Lorentzian to different balanced or unbalanced doublets [1]. On the other hand, during the transient regime, the DRUM undergoes its charging phase. As highlighted in section 3.2, equation 18 shows that the steady-state is determined solely by the final values of the intermodal coupling coefficients, regardless of the path followed during their evolution. Indeed, the transition from one initial set of coupling coefficients to another, may follow different trajectories, but the optical steady-state response depends only on the final values. This remains valid even if the variation of the coupling coefficients occurs during the charging phase of the DRUM. Such a process is related to the photon lifetime in the cavity, which is about 10 ps for a quality factor of the order of 10^4 [2]. Although difficult to achieve experimentally, such a scenario would lead to a different evolution of the optical field intensity during the transient phase, but still to the same final steady-state response independent of the trajectory followed.

It is important to note that in our model we set ϕ_{21} = 0 and $\phi_{12} = \phi_0$, since the equilibrium values depend on the sum of the two phases ($\phi_{12} + \phi_{21}$), as shown in equation 28. The choice of the initial phase value is therefore arbitrary, and we define it as zero for the resonance that exhibits a single Lorentzian lineshape in the default DRUM state (i.e., when no current is applied to the thermal heaters in the lobes). Under this condition, the values obtained from the fitting of the experimental lineshapes were approximately 50 GHz for both intermodal couplings, $|\beta_{12}|$ and $|\beta_{21}|$. See [1] for more details.

2 Nonlinear dynamics: equations of the DRUM

The time-dependent non-linear behavior of a silicon DRUM can be represented by a set of three coupled ordinary differential equations [3]. These equations describe the evolution of the optical fields (α_1 and α_2) within the microresonator, the free carrier concentration (ΔN) and the temperature difference between the waveguide core and the cladding (ΔT) [4, 3, 5]. By defining for simplicity $\alpha^2 = |\alpha_1|^2 + |\alpha_2|^2$,

$$\begin{aligned}
\frac{d\alpha_1}{dt} &= \left(i(\omega_{\text{r}} + \delta\omega_{\text{T}}\Delta\text{T} + \delta\omega_{\text{N}}\Delta\text{N} - \omega) - \frac{\gamma_{\text{loss}}\left(\alpha^2, \Delta\text{N}\right)}{2}\right)\alpha_1 - \beta_{21}\alpha_2 \\
\frac{d\alpha_2}{dt} &= \left(i(\omega_{\text{r}} + \delta\omega_{\text{T}}\Delta\text{T} + \delta\omega_{\text{N}}\Delta\text{N} - \omega) - \frac{\gamma_{\text{loss}}\left(\alpha^2, \Delta\text{N}\right)}{2}\right)\alpha_2 - \beta_{12}\alpha_1 + i\sqrt{\gamma_{\text{coup}}}E_{\text{in}} \\
\frac{d\Delta\text{N}}{dt} &= -\frac{\Delta\text{N}}{\tau_{\text{fc}}} + \text{N}_{a4}\left(|\alpha_1|^2 + |\alpha_2|^2\right)^2 \\
\frac{d\Delta\text{T}}{dt} &= -\frac{\Delta\text{T}}{\tau_{\text{th}}} + \left(|\alpha_1|^2 + |\alpha_2|^2\right)\text{T}_{a2}\left(\alpha^2, \Delta\text{N}\right),
\end{aligned} \tag{19}$$

where the total losses γ_{loss} and T_{a2} are the following functions of α and ΔN:

$$\begin{aligned}
\gamma_{\text{loss}}\left(\alpha^2, \Delta\text{N}\right) &= 5\gamma_{\text{coup}} + \gamma_{\text{rad}} + \gamma_{\text{abs,lin}} + g_{a2}\alpha^2 + g_{\text{N}}\Delta\text{N} \\
\text{T}_{a2}\left(\alpha^2, \Delta\text{N}\right) &= \frac{\Gamma_{\text{th}}\left(\gamma_{\text{abs,lin}} + g_{a2}\alpha^2 + g_{\text{N}}\Delta\text{N}\right)}{c_p\rho_{\text{si}}V_{\text{th}}},
\end{aligned} \tag{20}$$

with

$$g_{a2} = \frac{\Gamma_{\text{TPA}}\beta_{\text{Si}}c^2}{n_g^2 V_{\text{TPA}}}, \quad g_{\text{N}} = \frac{\Gamma_{\text{FCA}}\sigma_{\text{N}}c}{n_g}. \tag{21}$$

Finally, N_{a4} is defined as:

$$\mathrm{N}_{a4} = \frac{\Gamma_{\mathrm{FCA}}\beta_{\mathrm{Si}}c^2}{2\hbar\omega_r V_{\mathrm{FCA}}^2 n_g^2}, \tag{22}$$

The definition of the various constants in Eq. (19-22) and their values, as used in the simulations, are listed in table 1. They were primarily taken from [6]. The volumes, as well as the parameters $\frac{dn_{\mathrm{Si}}}{dN}$, σ_{Si}, γ_{coup}, τ_{th}, τ_{fc}, β_{12}, and β_{21}, were fine-tuned based on experimental data.

Table 1: Parameters employed for the simulations

Name	Symbol	Value
Resonant frequency	ω_r	$2\pi \times 193.069\,\mathrm{THz}$
TPA constant	β_{Si}	$8.4 \times 10^{-12}\,\mathrm{mW}^{-1}$
Thermo optic coefficient of silicon	$\frac{dn_{\mathrm{Si}}}{dT}$	$1.86 \times 10^{-4}\,\mathrm{K}^{-1}$
Frequency displacement factor due to temperature	$\delta\omega_{\mathrm{T}} = -\frac{\omega_r}{n_g}\frac{dn_{\mathrm{Si}}}{dT}$	$-0.065 \times 10^{-4}\,\mathrm{THz\ K}^{-1}$
Lumped Free carrier dispersion coefficient	$\frac{dn_{\mathrm{Si}}}{dN}$	$-3.46 \times 10^{-27}\,\mathrm{m}^3$
Frequency displacement factor due to free-carriers	$\delta\omega_{\mathrm{N}} = -\frac{\omega_r}{n_g}\frac{dn_{\mathrm{Si}}}{dN}$	$1.208 \times 10^{-24}\,\mathrm{THz\ m}^3$
Absorption cross-section	σ_{Si}	$1.5 \times 10^{-21}\mathrm{m}^2$
Silicon density	ρ_{Si}	$2.33\,\mathrm{g\,cm}^{-3}$
Silicon thermal capacity	$c_{\mathrm{p,Si}}$	$0.7\,\mathrm{J\,g}^{-1}\,\mathrm{K}^{-1}$
Refractive index of bulk silicon	$n_g = n_{\mathrm{Si}}$	3.476
Efficiency of linear absorption rate	$\eta_{\mathrm{lin}} = \frac{\gamma_{\mathrm{abs,lin}}}{\gamma_{\mathrm{abs,lin}}+\gamma_{\mathrm{rad}}}$	0.4
Linear absorption rate	$\gamma_{\mathrm{abs,lin}}$	$\frac{\eta_{\mathrm{lin}}}{102.5}\mathrm{THz}$
Coupling loss into the waveguide	γ_{coup}	$0.026\,\mathrm{THz}$
Thermal relaxation time	τ_{th}	$80\,\mathrm{ns}$
Free carriers relaxation time	τ_{fc}	$12\,\mathrm{ns}$
Thermal confinement factor	Γ_{th}	0.9355
TPA confinement factor	Γ_{TPA}	0.9964
FCA confinement factor	Γ_{FCA}	0.9996
Thermal effective volume	V_{th}	$44.66\,\mu\mathrm{m}^3$
TPA effective volume	V_{TPA}	$36.26\,\mu\mathrm{m}^3$
FCA effective volume	V_{FCA}	$33.04\,\mu\mathrm{m}^3$
Left-lobe intermodal coupling coefficient	$\lvert\beta_{12}\rvert$	$55 \times 10^{-3}\,\mathrm{THz}$
Right-lobe intermodal coupling coefficient	$\lvert\beta_{21}\rvert$	$65 \times 10^{-3}\,\mathrm{THz}$

3 Initial state recovery over forward and reverse phase sweeps

The condition of *path-dependent phase rotation* can be easily removed experimentally by switching the laser off and on between different scanned phase points. This procedure, combined with turning the laser off and on during the input wavelength tuning, ensures that each state or point is disconnected. We refer to this measurement approach as *path-independent phase rotation*. In this case there is no memory between one point and another, i.e. the system has no recollection of the path taken to reach a given phase and/or detuning wavelength state. Therefore, the results for a *forward* and a *reverse* sweep of the PSL must be equal.

Fig. 1 is analogous to Fig. 3 shown in subsection 3.2 of the main text. Specifically, maps (a) and (b) show the experimental SP frequency as a function of the phase applied by the PSL and the detuning wavelength, for a full-cycle *forward* and *reverse* sweep, respectively. Maps (c) and (d) show the corresponding theoretical results. Meanwhile, maps (e)-(f) and (g)-(h) show, using the same parameters, the behavior of the normalized experimental and theoretical average transmission, respectively. The SP frequency maps obtained for the two directions of PSL variation show comparable trends within the limits of the experimental error. Although they have the same overall shape, the initial states for the *forward* (0) and *reverse* (2π) sweeps are slightly different. In the *forward* mode, for negative detuning, the state exhibits SP oscillations; in the reverse case, it does not. A similar but opposite behavior occurs for a positive detuning of about 80 pm. This discrepancy is attributed to the red-shift induced by the current applied to the PSL, which slightly alters

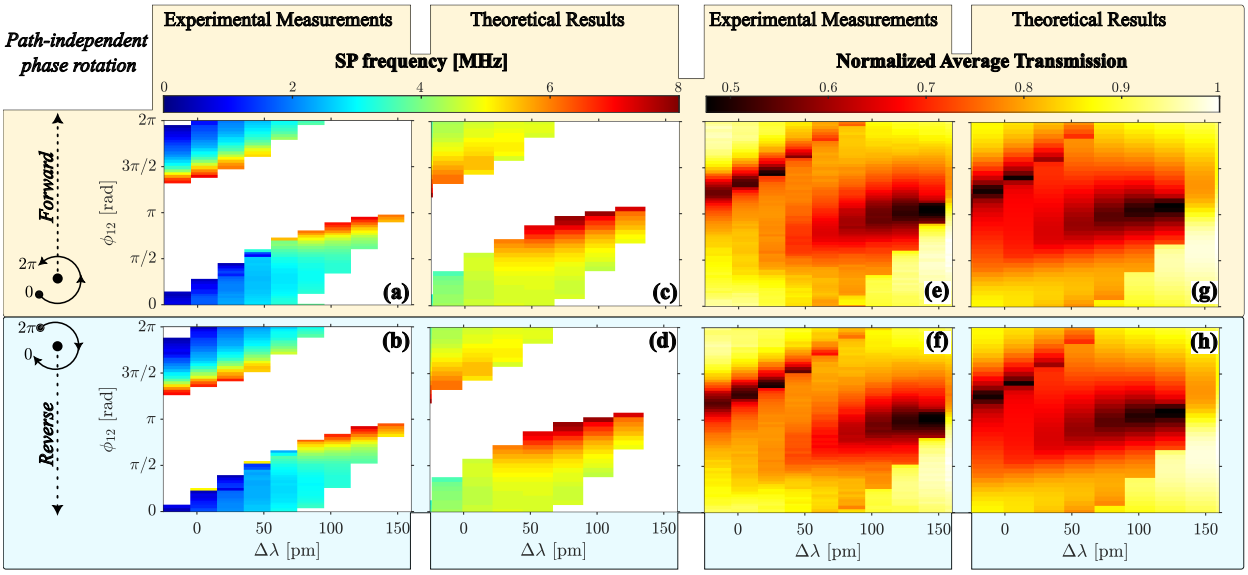

Figure 1: **Maps of SP frequency and normalized average optical response under full-cycle path-independent phase rotation.** (a)-(b) and (c)-(d): Experimental and simulated SP frequency as a function of wavelength detuning and phase applied via the phase shifter left. (e)-(f) and (g)-(h): Experimental and simulated normalized mean optical power for the same parameters. The top row ((a), (c), (e), (g)) corresponds to a full phase sweep from 0 to 2π (*forward*); the bottom row ((b), (d), (f), (h)) shows the *reverse* sweep from 2π to 0. In both cases, the system is reset to its initial state between steps, i.e. *path-independent phase rotations*.

the response of the system (see subsection 3.1 in the main text). However, it is important to note that the two maps (a) and (b) do not exhibit bistable states or hysteresis regimes, as observed in the *path-dependent* case presented in subsection 3.2 of the main text. The theoretical maps accurately reproduce the experimental behavior and show no difference between the two directions of phase variation. In particular, the experimental power maps (see maps (e) and (f)) are comparable, confirming the absence of memory between states. These are very accurately reproduced by the theoretical simulations shown in maps (g) and (h).

4 Equilibrium point analysis

In this subsection, we outline the procedure used to determine the equilibrium points of the DRUM, which involves defining the *refined nullclines*. Using the notation:

$$a \equiv \omega_{\mathrm{r}} + \delta\omega_{\mathrm{N}}\Delta\mathrm{N} + \delta\omega_{\mathrm{T}}\Delta\mathrm{T} - \omega, \quad b \equiv \frac{\gamma_{\mathrm{loss}}\left(\alpha^2, \Delta\mathrm{N}\right)}{2}, \tag{23}$$

the first two equations of the coupled system in Eq. 19 can be reformulated as:

$$\begin{aligned} \frac{d\alpha_1}{dt} &= (ia - b)\alpha_1 - \beta_{21}\alpha_2 \\ \frac{d\alpha_2}{dt} &= (ia - b)\alpha_2 - \beta_{12}\alpha_1 + i\sqrt{\gamma_{\mathrm{coup}}}E_{\mathrm{in}}. \end{aligned} \tag{24}$$

At equilibrium, we can set the time derivatives to zero. The equations for the free carriers and temperature in Eq.19 reduce to:

$$\begin{aligned} \Delta\mathrm{N}_{\mathrm{eq}} &= \tau_{\mathrm{fc}}\mathrm{N}_{a4}\left(|\alpha_1|^2 + |\alpha_2|^2\right)^2 \\ \Delta\mathrm{T}_{\mathrm{eq}} &= \tau_{\mathrm{th}}\mathrm{T}_{a2}\left(\alpha^2\,, \Delta\mathrm{N}_{\mathrm{eq}}\right)\left(|\alpha_1|^2 + |\alpha_2|^2\right), \end{aligned} \tag{25}$$

namely they are functions of $|\alpha_1|^2$, $|\alpha_2|^2$. Now let us set the derivatives in Eq.24 to zero:

$$\begin{aligned} 0 &= (ia - b)\alpha_1 - \beta_{21}\alpha_2 \\ 0 &= (ia - b)\alpha_2 - \beta_{12}\alpha_1 + i\sqrt{\gamma_{\mathrm{coup}}}E_{\mathrm{in}}. \end{aligned} \tag{26}$$

After some algebra, it is possible to write them as:

$$
\begin{aligned}
-iE_{\text{in}}\sqrt{\gamma_{\text{coup}}} &= \left(-\frac{\beta_{12}\beta_{21}}{ia-b}+ia-b\right)\alpha_2 \\
-iE_{\text{in}}\sqrt{\gamma_{\text{coup}}} &= \frac{(ia-b)\left(-\frac{\beta_{12}\beta_{21}}{ia-b}+ia-b\right)}{\beta_{21}}\alpha_1.
\end{aligned}
\tag{27}
$$

Now one can take the squared modulus of the Right-Hand Side (RHS) and Left-Hand Side (LHS) to achieve:

$$
\begin{aligned}
|E_{\text{in}}|^2\gamma_{\text{coup}} &= \left|-\frac{\beta_{12}\beta_{21}}{ia-b}+ia-b\right|^2|\alpha_2|^2 \\
|E_{\text{in}}|^2\gamma_{\text{coup}} &= \left|\frac{(ia-b)\left(-\frac{\beta_{12}\beta_{21}}{ia-b}+ia-b\right)}{\beta_{21}}\right|^2|\alpha_1|^2.
\end{aligned}
\tag{28}
$$

These are two functions of $|\alpha_1|^2$ and $|\alpha_2|^2$. Now, let us consider the two functions f_1 and f_2:

$$
\begin{aligned}
f_1 &= \left|-\frac{\beta_{12}\beta_{21}}{ia-b}+ia-b\right|^2|\alpha_2|^2-|E_{\text{in}}|^2\gamma_{\text{coup}} \\
f_2 &= \left|\frac{(ia-b)\left(-\frac{\beta_{12}\beta_{21}}{ia-b}+ia-b\right)}{\beta_{21}}\right|^2|\alpha_1|^2-|E_{\text{in}}|^2\gamma_{\text{coup}}.
\end{aligned}
\tag{29}
$$

They are not simply nullclines, since they are not the time derivatives of equation 24. We decided to call them *refined nullclines*. When they intersect in the $|\alpha_1|^2$, $|\alpha_2|^2$ space their intersection at ($|\alpha_1^{\text{eq}}|^2$, $|\alpha_2^{\text{eq}}|^2$) has the physical meaning of equilibrium point. One can find such an intersection numerically and then insert it into Eq.25 to find the equilibrium values of ΔN and ΔT.

5 Determination of the Eigenvalues

This subsection presents the eigenvalue analysis that was performed to determine the nature of the DRUM's equilibrium points. The system of equations 19 can be simplified by applying the adiabatic approximation [6]. Since the typical rate of change of α_1 and α_2 are much smaller than that of the free carriers and temperature, we may set the derivatives of the two modes to zero in the first two equations in the system of Eq.19. We end up with the remaining two equations of Eq.19 and two equations that describe the dependence of the two modes on ΔN and ΔT. We may find the intersection of these curves for a given ΔN and ΔT to find the corresponding energy values of the two modes. This trick allows us to deal with a 4×4 Jacobian for the modes (a complex 2×2) and a 2×2 Jacobian for the free carriers and temperature instead of a single 6×6. In the following we are interested in the 2×2:

$$
\widetilde{\mathcal{J}} = \begin{pmatrix} \mathcal{J}_{11} & \mathcal{J}_{12} \\ \mathcal{J}_{21} & \mathcal{J}_{22} \end{pmatrix} = \begin{pmatrix} \frac{\partial}{\partial\Delta\text{N}}\frac{d\Delta\text{N}}{dt} & \frac{\partial}{\partial\Delta\text{T}}\frac{d\Delta\text{N}}{dt} \\ \frac{\partial}{\partial\Delta\text{N}}\frac{d\Delta\text{T}}{dt} & \frac{\partial}{\partial\Delta\text{T}}\frac{d\Delta\text{T}}{dt} \end{pmatrix},
\tag{30}
$$

where the elements of the Jacobian are:

$$
\begin{aligned}
\mathcal{J}_{11} &= -\frac{1}{\tau_{\text{fc}}} + 2\text{N}_{a4}(|\alpha_2|^2 + |\alpha_1|^2)\frac{\partial}{\partial \Delta \text{N}}(|\alpha_2|^2 + |\alpha_1|^2) \\
\mathcal{J}_{12} &= 2\text{N}_{a4}(|\alpha_2|^2 + |\alpha_1|^2)\frac{\partial}{\partial \Delta \text{T}}(|\alpha_2|^2 + |\alpha_1|^2) \\
\mathcal{J}_{21} &= \frac{\Gamma_{\text{th}}}{c_p \rho_{\text{si}} V_{\text{th}}}\left(g_{\text{a2}}\frac{\partial}{\partial \Delta \text{N}}(|\alpha_2|^2 + |\alpha_1|^2) + g_N\right)(|\alpha_2|^2 + |\alpha_1|^2) + \text{T}_{a2}\frac{\partial}{\partial \Delta \text{N}}(|\alpha_2|^2 + |\alpha_1|^2) \\
\mathcal{J}_{22} &= -\frac{1}{\tau_{\text{th}}} + \left(\frac{\Gamma_{\text{th}}}{c_p \rho_{\text{si}} V_{\text{th}}}\left(g_{\text{a2}}\frac{\partial}{\partial \Delta \text{T}}\left(|\alpha_1|^2 + |\alpha_2|^2\right)\right)\left(|\alpha_1|^2 + |\alpha_2|^2\right)\right) + \\
&\quad \left(T_{\text{a2}}\frac{\partial}{\partial \Delta \text{T}}\left(|\alpha_1|^2 + |\alpha_2|^2\right)\right).
\end{aligned} \tag{31}
$$

The partial derivatives of $|\alpha_1|^2$, $|\alpha_2|^2$ with respect of ΔN and ΔT are required. One may insert first $\Delta\text{N}_{\text{eq}} + \delta\text{N}$ and $\Delta\text{T}_{\text{eq}}$ and then $\Delta\text{N}_{\text{eq}}$ and $\Delta\text{T}_{\text{eq}} + \delta\text{T}$ in Eq. 28 to find the intersection in the $|\alpha_1|^2$, $|\alpha_2|^2$ space to obtain:

$$
\begin{aligned}
&|\alpha_1(\Delta\text{N}_{\text{eq}} + \delta\text{N}, \Delta\text{T}_{\text{eq}})|^2, \quad |\alpha_2(\Delta\text{N}_{\text{eq}} + \delta\text{N}, \Delta\text{T}_{\text{eq}})|^2, \\
&|\alpha_1(\Delta\text{N}_{\text{eq}}, \Delta\text{T}_{\text{eq}} + \delta\text{T})|^2, \quad |\alpha_2(\Delta\text{N}_{\text{eq}}, \Delta\text{T}_{\text{eq}} + \delta\text{T})|^2.
\end{aligned} \tag{32}
$$

In this way, it is possible to evaluate:

$$
\begin{aligned}
\frac{\partial|\alpha_1(\Delta\text{N}_{\text{eq}}, \Delta\text{T}_{\text{eq}})|^2}{\partial \text{N}} &= \frac{|\alpha_1(\Delta\text{N}_{\text{eq}} + \delta\text{N}, \Delta\text{T}_{\text{eq}})|^2 - |\alpha_1(\Delta\text{N}_{\text{eq}}, \Delta\text{T}_{\text{eq}})|^2}{\delta\text{N}} \\
\frac{\partial|\alpha_2(\Delta\text{N}_{\text{eq}}, \Delta\text{T}_{\text{eq}})|^2}{\partial \text{N}} &= \frac{|\alpha_2(\Delta\text{N}_{\text{eq}} + \delta\text{N}, \Delta\text{T}_{\text{eq}})|^2 - |\alpha_2(\Delta\text{N}_{\text{eq}}, \Delta\text{T}_{\text{eq}})|^2}{\delta\text{N}} \\
\frac{\partial|\alpha_1(\Delta\text{N}_{\text{eq}}, \Delta\text{T}_{\text{eq}})|^2}{\partial \text{T}} &= \frac{|\alpha_1(\Delta\text{N}_{\text{eq}}, \Delta\text{T}_{\text{eq}} + \delta\text{T})|^2 - |\alpha_1(\Delta\text{N}_{\text{eq}}, \Delta\text{T}_{\text{eq}})|^2}{\delta\text{T}} \\
\frac{\partial|\alpha_2(\Delta\text{N}_{\text{eq}}, \Delta\text{T}_{\text{eq}})|^2}{\partial \text{T}} &= \frac{|\alpha_2(\Delta\text{N}_{\text{eq}}, \Delta\text{T}_{\text{eq}} + \delta\text{T})|^2 - |\alpha_2(\Delta\text{N}_{\text{eq}}, \Delta\text{T}_{\text{eq}})|^2}{\delta\text{T}},
\end{aligned} \tag{33}
$$

and from here, the eigenvalues are given by:

$$
\widetilde{\lambda}_{1,2} = \frac{1}{2}\left(\mathcal{J}_{11} + \mathcal{J}_{22} \mp \sqrt{\mathcal{J}_{11}^2 - 2\mathcal{J}_{22}\mathcal{J}_{11} + \mathcal{J}_{22}^2 + 4\mathcal{J}_{12}\mathcal{J}_{21}}\right). \tag{34}
$$

References

[1] Bulent Aslan, Riccardo Franchi, Stefano Biasi, Salamat Ali, Davide Olivieri, and Lorenzo Pavesi. Coherent control of (non-)hermitian mode coupling: tunable chirality and exceptional point dynamics in photonic microresonators. *Research Square Preprint*, 2025.

[2] Stefano Biasi, Pierre Guillemé, Andrea Volpini, Giorgio Fontana, and Lorenzo Pavesi. Time response of a microring resonator to a rectangular pulse in different coupling regimes. *Journal of Lightwave Technology*, 37(19):5091–5099, 2019.

[3] Thomas J Johnson, Matthew Borselli, and Oskar Painter. Self-induced optical modulation of the transmission through a high-q silicon microdisk resonator. *Optics express*, 14(2):817–831, 2006.

[4] Stefano Gretter, Mattia Mancinelli, and Lorenzo Pavesi. Dynamic analysis and reservoir computing application of a nonlinear microring resonator. *ACS Photonics*, 2025.

[5] Stefano Biasi, Riccardo Franchi, Davide Bazzanella, and Lorenzo Pavesi. On the effect of the thermal cross-talk in a photonic feed-forward neural network based on silicon microresonators. *Frontiers in Physics*, 10:1093191, 2022.

[6] Thomas Van Vaerenbergh, Martin Fiers, Pauline Mechet, Thijs Spuesens, Rajesh Kumar, Geert Morthier, Benjamin Schrauwen, Joni Dambre, and Peter Bienstman. Cascadable excitability in microrings. *Optics express*, 20(18):20292–20308, 2012.